Journal of
Environmental & Analytical Toxicology

Zhi-Chen et al., J Environ Anal Toxicol 2017, 7:3
DOI: 10.4172/2161-0525.1000450

Research Article Open Access

The Selective Catalytic Reduction of NOx Over Cd-Ce-Ti Metal Oxide Catalysts

Duan Zhi-Chen, Liu Jian*, Shi Juan, Zhao Zhen, Wei Yue-Chang, Li Jian-Mei, Zhang Xiao, Jiang Gui-Yuan and Duan Ai-Jun

State Key Laboratory of Heavy Oil Processing, Beijing Key Lab of Oil and Gas Pollution Control, China University of Petroleum, Beijing 102249, China

Abstract

The transition metal oxide Cd-Ce-TiO_2 catalysts were prepared by the method of coprecipitation. The catalysts were characterized by means of XRD, BET, SEM, TEM, Raman and UV-Vis DRS. And the catalytic activities of the catalysts for deNO_x were evaluated by NH_3-SCR reaction. The nanoparticles will be formed for Cd-$Ce_{0.2}$-TiO_x catalysts with the different metal Cd contents. The catalysts possess the irregular, mesoporous structure. XRD and Raman data demonstrated that at the low content of Cd, anatase structure disappeared in the catalyst, but the amorphous oxide was formed. And BET pore size distribution shows the formation of the mesoporous structure in the mixed-oxide. Among all the catalysts, 2% Cd-$Ce_{0.2}$-TiO_x catalyst exhibits the best NH_3-SCR performance with a wide temperature window from 225 to 525°C for NO conversion above 90%.

Keywords: NH_3-SCR; Catalyst; Cd-Ce-Ti oxide; Coprecipitation; Wide temperature window

Introduction

In recent years, the national standard to environment has become more and more strict, NO_x emissions need to be effectivly controlled [1,2]. The SCR of NO_x with NH_3 is nowadays considered as the most promising technology for the elimination of NO_x, whereas most of the commercial catalysts for this process are V_2O_5/TiO_2 promoted by WO_3 or MoO_3 [3-5]. Although these catalysts show highly catalytic activity for NO reduction, there are still some problems, which involve high activity for oxidation of SO_2 to SO_3, the formation of N_2O at high temperatures and toxicity of vanadia. SO_3 produced by the oxidation of SO_2 reacts with NH_3 and H_2O to form NH_4HSO_4, $(NH_4)_2S_2O_7$, and H_2SO_4, which cause equipment corrosion and catalyst pore plugging. N_2O contributes to greenhouse effects and the destruction of ozone layer [6,7]. For the above reasons, there has been strong interest in developing new SCR catalysts with high activity and selectivity for NO removal [8-10].

Recently, the nontoxic and inexpensive material, ceria (CeO_2) has attracted large attention in catalysis mainly due to its prominent ability to store/release oxygen as an oxygen reservoir via the redox shift between Ce^{4+} and Ce^{3+} under oxidizing and reducing conditions, respectively. The presence of ceria enhanced the oxidation of NO to NO_2, thereby increasing the activity of NO reduction [11-13]. However, pure ceria is known to be poorly thermostable and undergo rapid sintering at higher temperatures, thereby losing oxygen storage capacity (OSC). It would lead to the deactivation of the catalysts [14,15]. The transition metal Cd, has attracted attention in environmental catalysis, such as photocatalysis and hydrodesulfurization [16]. However, there is lack to study for NO_x reduction. By the incorporation of metal oxide Cd into the ceria lattice, it is beneficial to the formation of mixed oxides or solid solutions. In this work, Cd-$Ce_{0.2}$-TiO_x catalysts were prepared with different Cd contents for improving the catalytic performances for the SCR of NO with NH_3. Their physicochemical properties were investigated systematically.

Experimental

Catalyst preparation

A series of Cd-$Ce_{0.2}TiO_x$ catalysts with fixed Ce/Ti molar ratio of 0.2 and Cd/Ti molar ratio of 0, 1%, 2%, 3%, 4%, 5% were prepared by the coprecipitation method. All chemicals were of analytical grade.

In a typical synthesis, a series of stoichiometric solution (100 mL) of $Ti(SO_4)_2$ and $Ce(NO_3)_2$ was prepared, the required amount of $Cd(CH_3COO)_2$ was added to the solution at stirring, then NH_3-H_2O solutions was slowly dropped into the solution of Cd-Ce-Ti under vigorous agitation until pH = 10. And then the suspension was aged in air for 24 h at room temperature and atmospheric pressure.

The precipitation was filtered, and dried at 100 °C for 12 h, and consequently calcined in air at 500°C for 6 h. The final catalyst was labeled as M% Cd-$Ce_{0.2}TiO_x$ (M = 0, 1%, 2%, 3%, 4%).

Catalyst characterization

Powder XRD patterns were obtained by a powder X-ray diffractometer (Shimadzu XRD 6000) using Cu Kα (λ= 0.15406 nm) radiation with a Nickel filter operating at 40 kV and 10 mA in the 2θ range of 5-70° at a scanning rate of 4°/min.

UV-Vis diffuse reflectance spectroscopy (UV-Vis DRS) experiments were performed on a UV-Vis spectrophotometer (Hitachi U-4100) with the integration sphere diffuse reflectance attachment. N_2 adsorption-desorption isotherm was measured at 77 K using a Micromeritics TriStar II 2020 porosimetry analyzer. The samples were degassed at 300°C for 8 h prior to the measurements. The specific surface areas were calculated according to the Brunauer-Emmett-Teller (BET) method.

Raman spectra was measured at room temperature and excitation at 532 nm by using HR800 He-Gd laser (France HoribaJobin Yvon company) as the light source, with OMA - III detector (American Princefin Applied Research company). The Raman spectra of sample were recorded in the range of 100 ~ 900 cm^{-1}.

The surface morphology of the catalyst was observed by field emission scanning electron microscopy (FESEM) on a Quanta 200F

***Corresponding author:** Liu Jian, State Key Laboratory of Heavy Oil Processing, Beijing Key Lab of Oil and Gas Pollution Control, China University of Petroleum, Beijing 102249, China, Tel: 861089732278; Fax: 861069724721; E-mail: liujian@cup.edu.cn

Received March 15, 2017; **Accepted** March 23, 2017; **Published** April 04, 2017

Citation: Zhi-Chen D, Jian L, Juan S, Zhen Z, Chang WY, et al. (2017) The Selective Catalytic Reduction of NOx Over Cd-Ce-Ti Metal Oxide Catalysts. J Environ Anal Toxicol 7: 450. doi: 10.4172/2161-0525.1000450

instruments using accelerating voltages of 5 kV, in combination with an EDAX genesis 4000 energy-dispersive X-ray spectrometer (EDX). The TEM images were carried out using a JEOL JEM 2100 electron microscope equipped with a field emission source at an accelerating voltage of 200 kV.

Temperature-programmed reduction with H_2 (H_2-TPR) measurements were performed in a conventional flow apparatus. 100 mg sample was pretreated under air atmosphere by calcination at 300°C for 1 h and subsequently cooled to 30°C. Afterwards, 10% H_2/Ar flow (40 mL/min) was passed over the catalyst bed while the temperature was ramped from 30 to 600°C at a heating rate of 10°C/min.

Catalytic activity measurement

NH_3-SCR activity measurements were carried out in a fixed bed quartz micro-reactor operating in a steady flow mode. 0.4 g of catalysts were sieved with 40-60 mesh and used in each test. The reactant gas included 1000 ppm NO, 1000 ppm NH_3, 3% O_2 and balance N_2. The total flow rate was 500 mL/min and thus a GHSV of 45 000 h^{-1} was obtained. The temperature varied from 100 to 500°C, and heating rate was 3°C/min. The data was recorded when the temperature held at each point for more than 5 min. The concentration of NO_x (NO_x = NO + NO_2) in the inlet and outlet gas mixture was measured by a SIGNAL 4000 VM NO_x analyzer. Meanwhile, the concentration of NH_3, NO, NO_2 and N_2O were measured by a FTIR spectrometer (MKS, MultiGas 2030HS).

NO conversion and N_2 selectivity are calculated in the following equations (1) and (2).

$$\text{NO Conversion} = \frac{[NO]_{inlet} - [NO]_{outlet}}{[NO]_{inlet}} \times 100\% \quad (1)$$

$$N_2 \text{ Selectivity} = \left(1 - \frac{2[N_2O]_{outlet}}{[NO_x]_{inlet} + [NH_3]_{inlet} - [NO_x]_{outlet} - [NH_3]_{outlet}}\right) \times 100\% \quad (2)$$

Results and Discussion

XRD results

Figure 1 shows XRD patterns of M% Cd-$Ce_{0.2}TiO_x$ (M=0, 2, 3, 4) mixed-oxide catalysts calcined at 500°C. Crystalline phases are identified in comparison with ICDD files (anatase TiO_2, 21-1272; CeO_2, 34-0394), and anatase is a dominant characteristic in $Ce_{0.2}TiO_x$. As shown in Figure 1, the diffraction peaks at 25.4°, 47.6° are ascribed to the characteristic reflections of anatase TiO_2 and the peak at 28.6° is ascribed to fluorite CeO_2. There is no peak at 27.5° in the samples, which indicates that there is no rutile titania existing in all samples [17,18]. Moreover, no obvious characteristic peak assigned to a particular phase oxide is observed in 2% and 3% samples, which indicates that the amorphous phase was formed and become dominant phase in the samples [19]. This means that appropriate transition metal Cd facilitates the formation of amorphous mixed oxides. There is only one peak assigned to Cd oxide (peak at 32.12°) in 4% [20]. This means these transition metal oxides are well dispersed over $Ce_{0.2}TiO_x$ support for low Cd content samples.

N_2 adsorption-desorption results

Figure 2 and Table 1 exhibit the results of nitrogen adsorption-desorption isotherms and pore size of different samples calculated by the BJH method based on the N_2 adsorption-desorption isotherms. From Figure 2, the isotherms curves of 2%, 3% samples are typical type IV adsorption-desorption isotherms, which show that the mesoporous structure of the mixed-oxide, and the pore distribution is concentrated. The isotherms curves of 0%, 4% samples show that there were few mesoporous structure formed, and indicate that a small amount of metal Cd is helpful for the formation of mesoporous, but excess is harmful. 2% Cd-$Ce_{0.2}TiO_x$ exhibits higher specific surface area than 3% Cd-$Ce_{0.2}TiO_x$. It indicates that with the increasing of Cd content, there were more aggregation or blocks of nanoparticle. Table 1 shows that 2% and 3% samples contain mesopores with a relatively uniform pore size around 7 nm, and there were few mesopores in 0% and 4% samples. It may be assumed that the loading of Cd significantly affects on the structure of the catalysts.

XRD and BET results show that the SCR activity is combined with mesopore and amorphous state in this study. After adding moderate amount of Cd, the catalyst show high SCR performance. When adding excess content of Cd, the SCR performance was rapid down, and anatase titanium phase and agglomeration of nanoparticles were found in these catalysts. Moderate amount of Cd oxide may improve the dispersion of Ce-Ti species so that the catalyst disperses more evenly.

SEM and TEM results

Figure 3 show SEM images of the catalysts with the different Cd contents catalysts. Figure 3a shows that $Ce_{0.2}TiO_x$ sample is composed of irregularly localized, distinct edge within the relative regular geometry (nanoparticles). This is changed in the morphology of $Ce_{0.2}TiO_x$ samples after Cd impreganation. Less agglomeration and smaller particles are found, as shown in Figure 3b-3d, which produce those smaller particles and the higher surface area among these catalysts. The characterization results are consistent with previous BET results. As the pore-forming agent was not used during the catalyst preparation, it can speculate that hysteresis loop in nitrogen adsorption-desorption isotherm should be ascribed to the intergranular pores from nanoparticle-accumulation.

The morphology of the catalysts changed with the different Cd contents. As shown in Figure 3b, 3c, after adding a small amount of Cd, samples contain nanoparticles with a relatively uniform size and the

Sample	S_{BET} (m^2/g)	Dp (nm)	Vp (cm^3/g)
0% Cd-$Ce_{0.2}TiO_x$	29.0	9.8	0.15
2% Cd-$Ce_{0.2}TiO_x$	154.3	6.6	0.36
3% Cd-$Ce_{0.2}TiO_x$	80.0	7.7	0.25
4% Cd-$Ce_{0.2}TiO_x$	15.4	7.8	0.07

[a]Calculated by BET method; [b]Calculated by *t*-plot method

Table 1: Structural Parameters of the Cd-Ce-Ti oxide catalysts.

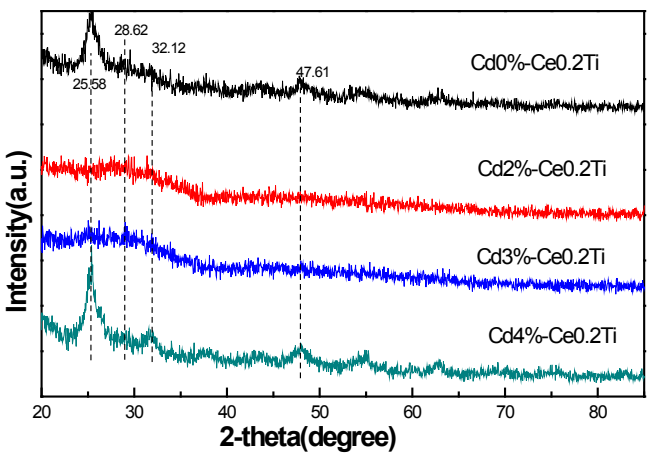

Figure 1: Bench-scale EC reactor with bipolar electrodes in parallel connection. (1) Electrocoagulation cell; (2) Anode; (3) Cathode; (4) bipolar electrodes; (5) Magnetic stirrer controlled; (6) Magnetic stirrer bar; (7) D.C. power supply.

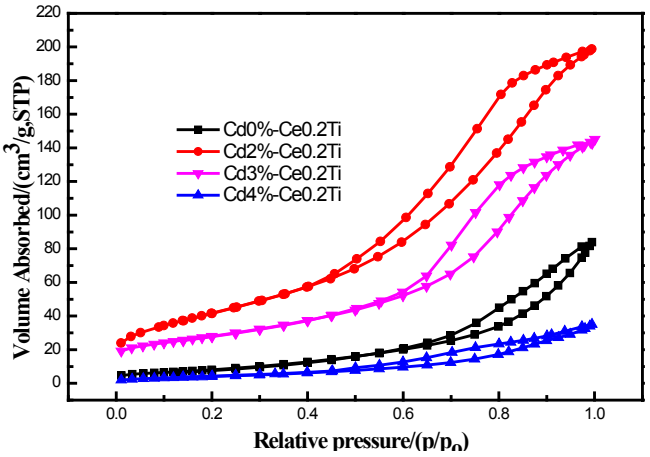

Figure 2: Nitrogen adsorption-desorption isotherms of the Cd-Ce-Ti oxide catalysts.

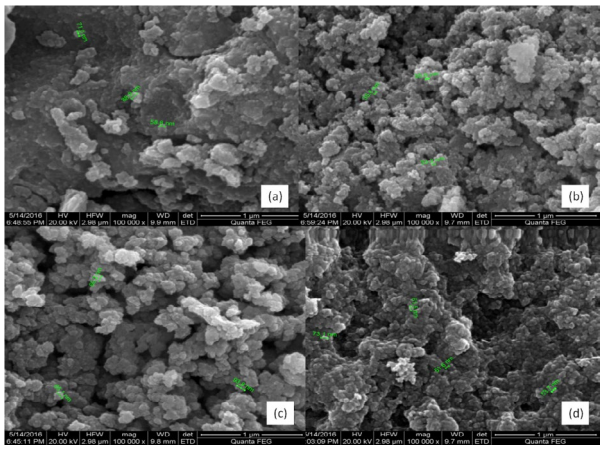

Figure 3: SEM images of different Cd content catalysts: (a) $Ce_{0.2}$-TiOx (b) 2% Cd-$Ce_{0.2}$-TiOx (c) 3% Cd-$Ce_{0.2}$-TiOx, (d) 4% Cd-$Ce_{0.2}$-TiOx.

structure is regular. Figure 3d shows that when adding excess Cd, there is obvious agglomeration and bigger particle size in samples.

TEM images of M% Cd-$Ce_{0.2}TiO_x$ (M=0, 2, 4) mixed-oxide catalysts are shown in Figure 5. The nanoparticle structure with overlapped pores can be clearly observed by TEM images. As shown in Figure 4, all samples display an irregular porous structure, corresponding to result of Figure 2. Ce-Ti nanocomposites show an irregular distribution and small particle sizes. The average particle size is 20 nm for Cd-Ce-Ti nanocomposites. As shown in Figure 4a, particles are found with the size above 150 nm in $Ce_{0.2}TiO_x$. Much smaller particles are found after Cd impreganations, as shown in Figure 4b. It leads to the higher surface area among these catalysts. The diffraction spot is obvious halo in SADE pattern (Figure 4b) of 2% Cd-$Ce_{0.2}TiO_x$, I indicates that the amorphous state is formed and become dominant phase in samples. Meanwhile, after loading excess Cd (Figure 4c, 4d), the particles become bigger, and they also possess the lower surface areas. In Figure 4d, the trace TiO_2 (0.35nm-TiO_2-101-anatase) clusters were distinguished [21]. SEM and TEM results show that the catalyst particles distribute uniformly with a certain particle size distribution.

UV-Vis DRS results

UV-Vis DRS spectroscopy was applied to understand the nature and coordination of cerium and titanium species in the samples. Figure 5 shows UV-Vis absorption spectra of M% Cd-$Ce_{0.2}TiO_x$ catalysts (M=0, 2, 3, 4). The bands at about 350 nm are assigned to anatase titania. For 2% and 3% samples, the wavenumber is red shifted to the visible-light region, and the absorption intensity aslo increases. It shows the enhancement of the charge moving between the conduction band and the valence band of TiO_2 and CeO_2 [22]. Moreover, the wavenumber of excess Cd loading (4%) is similar to $Ce_{0.2}TiO_x$ samples. This demonstrates that only the moderate metal Cd is well dispersed over $Ce_{0.2}TiO_x$, thus reducing the width of forbidden region of TiO_2. UV-Vis DRS results show that the wavenumber is red shifted to the visible-light region by loading Cd, thus reducing the width of forbidden region of TiO_2. It indicated that the catalyst may possess the better catalytic performance at low temperature after loading transition metal.

Raman results

Raman spectra with excitation at 532 nm of Cd-$Ce_{0.2}$-TiO_x catalysts have displayed in Figure 6. Based on the spectra, 2, 3% Cd-$Ce_{0.2}$-TiO_x samples do not offer distinct vibration peak, but one unconspicuous peak of 143 cm^{-1} is attributed to anatase TiO_2, thus amorphous phase become dominant state in samples. For the catalyst 4% Cd-$Ce_{0.2}$-TiO_x, the Raman peaks located at 143, 194, 395, 512, 640 cm^{-1} are associated with anatase TiO_2. Raman peaks located at 468 cm^{-1} is assigned to fluorite ceria, but it's not obvious, and there is no vibration peak assigned to Cd oxide [23,24]. This means that Cd is well dispersed over $Ce_{0.2}TiO_x$ support. This is consistent with XRD result.

NH_3-SCR activity

NO_x conversion as a function of reaction temperatures for M% Cd-$Ce_{0.2}TiO_x$ catalysts is showed in Figure 7. NO_x conversion changes with the increasing of reaction temperature over all the samples. $Ce_{0.2}TiO_x$ show a low catalytic activity. After adding suitable amount of cadmium, the catalytic activity has been significantly improved. As shown in Figure 7, NO conversion increases after the loading of Cd.

2% Cd-$Ce_{0.2}TiO_x$ catalyst shows the best catalytic performance with NO_x conversion above 90% from 225 to 525°C. The temperature window of 2% Cd-$Ce_{0.2}TiO_x$ shifts towards the low temperature range. NO_x conversion is rapid down for the high Cd content catalysts. Among all the catalysts tested in this study, 2% Cd-$Ce_{0.2}TiO_x$ catalyst exhibits the widest temperature window for the removal of NO_x.

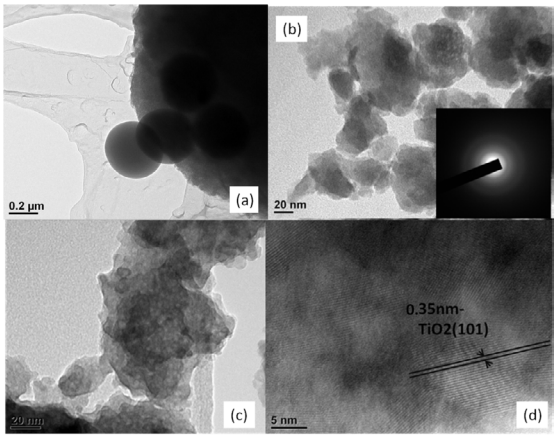

Figure 4: TEM images of different Cd contents catalysts: (a) $Ce_{0.2}$-TiO_x (b) 2% Cd-$Ce_{0.2}$-TiO_x (c, d) 4% Cd-$Ce_{0.2}$-TiO_x.

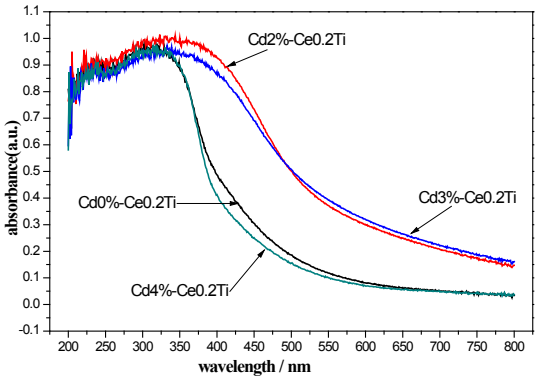

Figure 5: UV-Vis DRS of Ce-TiO_2 catalysts with varying Cd contents.

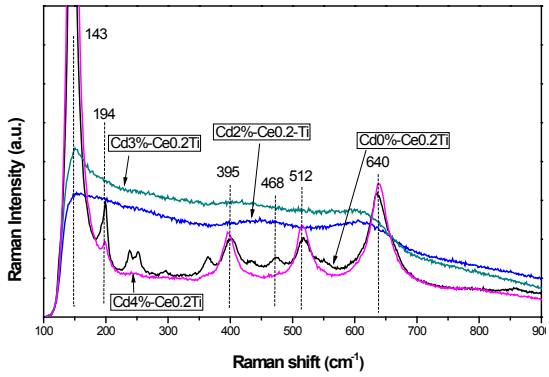

Figure 6: Raman spectra with excitation at 532 nm of Cd-$Ce_{0.2}$-TiO_x catalysts.

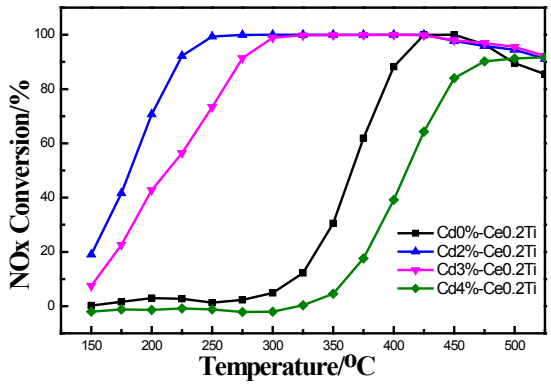

Figure 7: NO conversion as a function of reaction temperature over Ce-TiO_2 catalysts with different Cd contents.

Figure 8 shows the results of N_2 selectivity in NH_3-SCR reactions over 2% Cd-$Ce_{0.2}TiO_x$ catalysts in the temperature range of 150-525°C. As the temperature goes up, N_2 selectivity for 2%Cd-$Ce_{0.2}TiO_x$ decreases slightly. And 2% Cd-$Ce_{0.2}TiO_x$ exhibit the highest N_2 selectivity at 350°C.

The contents of cadmium oxide play important roles in affecting NH_3-SCR catalytic activity of those catalysts, and there is an optimal content of Cd. In this series of catalysts, 2% Cd-$Ce_{0.2}TiO_x$ not only exhibits good low temperature performance, but also gives a good N_2 selectivity throughout the reaction temperature range. In consideration of the highly catalytic activity and lack of study about Cd oxide used in SCR catalyst, further research may be carried out.

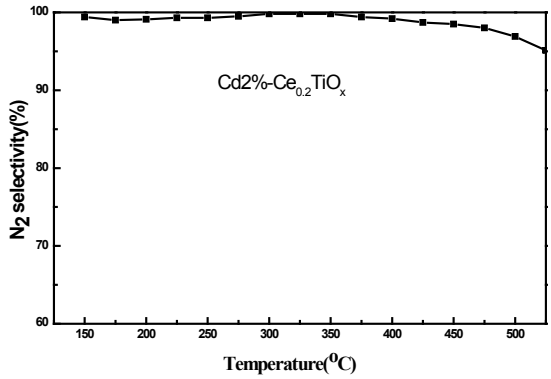

Figure 8: N_2 selectivity as a function of reaction temperature over 2%Cd-Ce0.2TiO_x catalyst.

Conclusions

Cd-Ce-Ti mixed-oxides were prepared by the coprecipitation method, and Cd oxides could be well dispersed over the samples. The different Cd contents in the catalysts change the specific surface area and the anatase phase of the mixed-oxide. When Cd contents are 1-3% in the catalysts, the amorphous phase are formed. The moderate cadmium oxide catalyst gives the highest low-temperature activity and N_2 selectivity. In the temperature range of 225~525°C, NO_x conversion exceeds 90% and N_2 selectivity is kept above 95% over 2% Cd-$Ce_{0.2}TiO_x$ catalyst.

Acknowledgements

This work was financially supported by the National Natural Science Foundation of China (21673290, 1162103 and 21376261), the National Hi-Tech Research and Development Program (863) of China (2015AA034603), and the China Offshore Oil Fund (LHYJYKJSA2016002).

References

1. Schultz MG, Diehl T, Brasseur GP, Zittel W (2003) Air pollution and climate-forcing impacts of a global hydrogen economy. Science 302: 624-627.
2. Liang Q, Zhao Z, Liu J, Wei YC, Jiang GY, et al. (2014) Pd Nanoparticles Deposited on Metal-Organic Framework of MIL-53(Al): an Active Catalyst for CO Oxidation, Acta Phys Chim. Sin 30: 129-134.
3. Tomita A, Yoshii T, Teranishi S, Nagao M, Hibino T (2007) Selective catalytic reduction of NOx by H2 using proton conductors as catalyst supports. Journal of Catalysis 247: 137-144.
4. Zhao X, Huang L, Li HR, Hu H, Han J, et al. (2015) Highly dispersed V2O5/TiO2 modified with transition metals (Cu, Fe, Mn, Co) as efficient catalysts for the selective reduction of NO with NH3. Chinese Journal of Catalysis 36: 1886-1899.
5. Zhao K, Han WL, Tang ZC, Zhang GD, Lu JY, et al. (2016) Investigation of coating technology and catalytic performance over monolithic V2O5-WO3/TiO2 catalyst for selective catalytic reduction of NOx with NH3. Colloids and Surfaces A: Physicochemical and Engineering Aspects 503: 53-60.
6. Cheng K, Liu J, Zhao Z, Wei YC, Jiang GY, et al. (2015) Direct synthesis of V-W-Ti nanoparticle catalysts for selective catalytic reduction of NO with NH3. RSC Advances 5: 45172-45183.
7. He H, Liu FD, Yu YB, Shan WP (2012) Environmental-friendly catalysts for the selective catalytic reduction of NOx Science China. Chemistry 42: 442-468.
8. Ettireddy PR, Ettireddy N, Mamedov S, Boolchand P, Smimiotis PG (2007) Surface characterization studies of TiO2 supported manganese oxide catalysts for low temperature SCR of NO with NH3. Applied Catalysis B: Environmental 76: 123-134.
9. Huang JH, Tong ZQ, Huang Y, Huang Y, Zhang JF (2008) Selective catalytic reduction of NO with NH3 at low temperatures over iron and manganese oxides supported on mesoporous silica. Applied Catalysis B: Environmental 78: 309-314.

10. Bai SL, Lu WH, Li DQ, Li XN, Fang YY, et al. (2014) Synthesis of Mesoporous TiO2 Microspheres and Their Use as Scattering Layers in Quantum Dot Sensitized Solar Cells. Acta Phys. Chim. Sin. 30: 1107-1112.

11. Liu ZM, Zhang SX, Li JH (2014) Novel V2O5-CeO2/TiO2 catalyst with low vanadium loading for the selective catalytic reduction of NOx by NH3. Appl. Catal. B- Environ. 158: 11-19.

12. Liu ZM, Zhang SX, Li JH, Ma LL (2014) Promoting effect of MoO3 on the NOx reduction by NH3 over CeO2/TiO2 catalyst studied with in situ DRIFTS. Appl. Catal. B-Environ 144: 90-95.

13. Xu C, Liu J, Zhao Z, Yu F, Cheng K, et al. (2015) NH3-SCR denitration catalyst performance over vanadium-titanium with the addition of Ce and Sb. J Environ Sci (China) 31: 74-80.

14. Lian Z, Liu F, He H (2014) Effect of preparation methods on the activity of VOx/CeO2 catalysts for the selective catalytic reduction of NOx with NH3. Catalysis Science & Technology 5: 389-396.

15. Wang R, Lan L, Gong MC, Chen YQ (2016) Catalytic Combustion of Gasoline Particulate Soot over CeO2-ZrO2 Catalysts. Acta Phys Chim Sin 32: 1747-1757.

16. Cui XF, Wang YJ, Jiang GY, Xu C, Duan AJ, et al. (2014) The Encapsulation of CdS into Carbon Nanotube for Stable and Efficient Photo catalysis. Journal of Materials Chemistry A 2: 20939-20946.

17. Wang W, Wang SP, Ma XB, Gong JL (2009) Crystal structures, acid–base properties, and reactivities of Cex Zr1- xO2 catalysts. Catalysis Today 148: 323-328.

18. Li P, Xin Y, Li Q, Wang ZP, Zhang ZL, et al. (2012) Ce-Ti amorphous oxides for selective catalytic reduction of NO with NH3: confirmation of Ce-O-Ti active sites. Environmental Science & Technology 46: 9600-9605.

19. Li Q, Gu HC, Li P, Zhou YH, Liu Y, et al. (2014) In situ IR studies of selective catalytic reduction of NO with NH3 on Ce-Ti amorphous oxides. Chinese Journal of Catalysis 35: 1289-1298.

20. Zhao GL, Yang YJ, Ren TZ (2006) Preparation of cadmium oxide nanoparticles. Acta Petrolei Sinica (Petroleum Processing Section) 22: 308-311.

21. Wang HQ, Cao S, Zheng F, Yu FX, Liu y, et al. (2015) CeO_2, doped anatase TiO_2, with exposed (001) high energy facets and its performance in selective catalytic reduction of NO by NH_3. Applied Surface Science 330: 245-252.

22. Lu XW, Li XZ, Qian JC, Miao NM, Yao C, et al. (2016) Synthesis and characterization of CeO2/TiO2 nanotube arrays and enhanced photocatalytic oxidative desulfurization performance. Journal of Alloys and Compounds 661: 363-371.

23. Li L, Hu GS, Lu JQ, Luo MF (2012) Review of Oxygen Vacancies in CeO2-doped Solid Solutions as Characterized by Raman Spectroscopy. Acta Phys Chim Sin 28: 1012-1020.

24. Choi HC, Jung YM, Kim SB (2005) Size effects in the Raman spectra of TiO_2 nanoparticles. Vibrational Spectroscopy 37: 33-38.